

RESEARCH

Open Access



# Strut-and-Tie Method for GFRP-RC Deep Members

Zahid Hussain<sup>1\*</sup> and Antonio Nanni<sup>1</sup>

## Abstract

The current code provisions in ACI 440.11 are based on the flexural theory that applies to slender members and may not represent the actual structural behavior when the shear span-to-reinforcement depth ratio is less than 2.5 (i.e., deep members). The Strut-and-tie method (STM) can be a better approach to design deep members; however, this chapter is not included in the code. Research has shown that STM models used for steel-reinforced concrete (RC) give satisfactory results when applied to glass fiber-reinforced polymer-reinforced (GFRP)-RC members with  $a/d$  less than 2.5. Therefore, this study is carried out to provide insights into the use of STM for GFRP-RC deep members based on the available literature and to highlight the necessity for the inclusion of a new chapter addressing the use of STM in the ACI 440.11 Code. It includes a design example to show the implications of ACI 440.11 code provisions when applied to GFRP-RC deep members (i.e., isolated footings) and compares it when designed as per STM provided in ACI 318-19. It was observed that current code provisions in ACI 440.11 required more concrete thickness (i.e.,  $h = 1.12$  m) leading to implementation challenges. However, the required dimensions decreased (i.e.,  $h = 0.91$  m) when the design was carried out as per STM. Due to the novelty of GFRP reinforcement, current code provisions may limit its extensive use in RC buildings, particularly in footings given the water table issues and excavation costs. Therefore, it is necessary to adopt innovative methods such as STM to design GFRP-RC deep members if allowed by the code.

**Keywords** GFRP, Reinforced concrete, Footing, Shear, Strut-and-tie method, Building code

## 1 Introduction

Reinforced concrete (RC) column footings are substructures that play an important role in transferring the superstructure load to the soil. Three different failure modes are usually considered in current practice when designing an isolated column footing which typically does not include shear reinforcement. First, one-way shear which is resisted by a single cross-section plane at a distance “ $d$ ” from the column face. Second is punching or two-way shear which is resisted along the perimeter

cross-section around the column at a distance “ $d/2$ ” from its faces. Third is flexure based on the Euler–Bernoulli beam theory. The building codes usually treat the design of isolated footings with the same provisions as those for elevated slabs. However, footings may behave differently due to their geometrical dimensions and varying soil pressure underneath (i.e., depending upon the type of soil). Hence, the direct application of code provisions for elevated slabs to footings may result in over-conservative and in some instances impractical designs.

ACI 440.11-22 (ACI, 2022) is a milestone for practitioners interested in the use of non-metallic reinforcement. However, the direct application of code provisions for one-way and two-way shear to footings makes the design difficult and implementation challenging. In the case of shallow foundations where shear reinforcement is not provided in usual practice, shear strength is provided

Journal information: ISSN 1976-0485 / eISSN 2234-1315.

\*Correspondence:

Zahid Hussain  
zxh446@miami.edu

<sup>1</sup> Civil and Architectural Engineering Department, University of Miami, Florida 33146, USA

solely by concrete and becomes the function of the member thickness. The current code requirements for shear in ACI 440.11-22 (ACI, 2022) were derived based on the neutral axis depth of a cracked transformed RC section, differently from ACI 318-19, which depends on the effective RC cross-section (ACI, 2019). The equations are further dependent on the axial stiffness of GFRP reinforcement. Since GFRP reinforcement has lower stiffness than steel, the shear design of GFRP-RC members requires more concrete thickness than steel-RC. This becomes challenging when applied to deep members such as footings. Therefore, optimizing the GFRP-RC footing design methods is necessary to make GFRP reinforcement a suitable sustainable material for replacing steel in reinforced concrete footings.

Structural members can be divided into beam-like regions (B-regions), where plane sections remain plane (i.e., assumptions of straight-line strain distribution apply), and disturbed regions (D-regions) where plane sections do not remain plane after the application of load. The Euler–Bernoulli beam theory of RC flexure and the

traditional approach ( $V_c + V_s$ ) for shear applies only to B-regions. In D-regions, however, compressive stresses are directly transferred to the supports rather than shear stresses as in the case of slender beams (Macgregor, 2002); therefore, a different design approach is warranted. The transfer mechanism formed in deep members resembles a hypothetical truss consisting of concrete struts subjected to compression, and steel ties resisting tension connected at joints referred to as nodes, such a configuration is known as a strut-and-tie model (STM). Collins and Mitchell, (1991) established a boundary between B-regions and D-regions and stated that STM controlled the shear strength of members with shear span-to-reinforcement depth ratio ( $a/d$ ) less than 2.5, beyond this limit sectional model controlled the behavior as given in Fig. 1 (Collins and Mitchell, 1991).

An experimental study reported that the flexural theory approach to design RC members was excessively conservative when applied to deep members such as pile caps. Whereas STM was found to be a more practical method as it considers the complete flow of forces rather

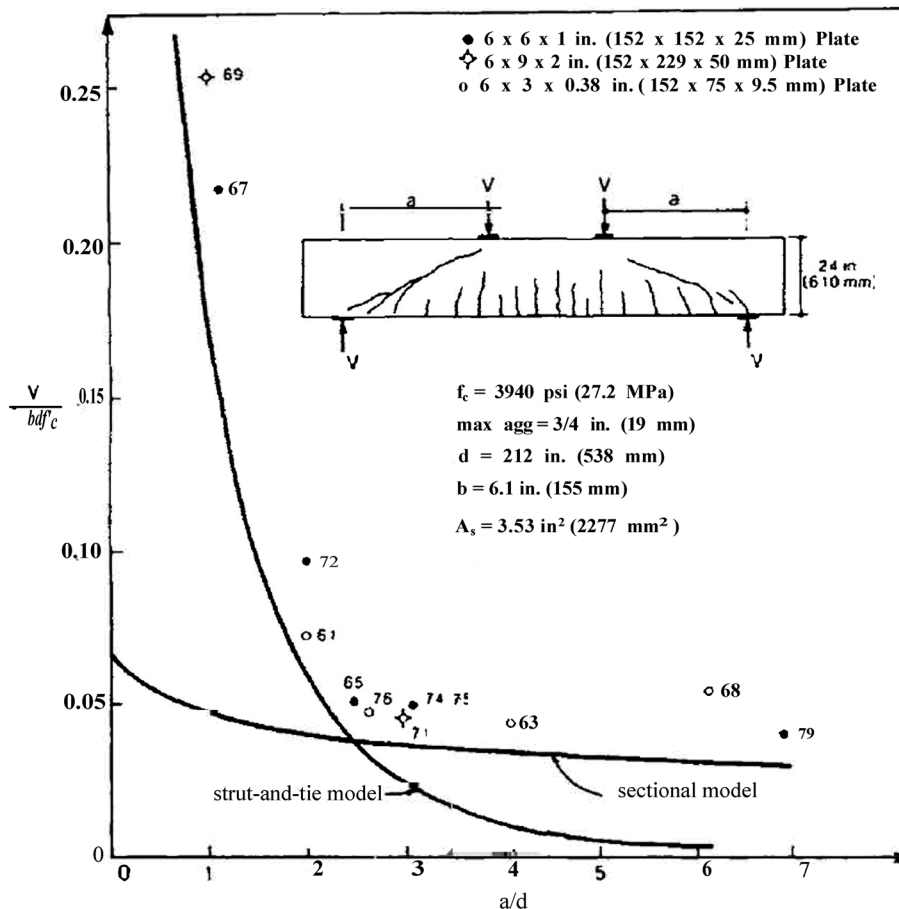


Fig. 1 Strength of concrete failing in shear for various a/d ratios (Collins et al. 1991)

than forces at a particular section (Adebar et al., 1996). Due to the novelty of GFRP material, the shear equations in ACI 440.11-22 (ACI, 2022) require bigger cross-sections and may not represent the actual flow of forces in the deep members, therefore, it is reasonable to design GFRP-RC footings using STM when  $a/d$  is less than 2.5 to minimize the thickness.

Most design codes including CSA S806-12 (CSA, 2012) for GFRP-RC allow the design of deep members using STM but the current edition of ACI 440.11-22 Building code (ACI, 2022) is silent on this topic. CSA S806-12 introduced the STM for FRP-RC deep beams, which is the same model specified in CSA A23.3 for steel-reinforced deep beams. The effect of lower elastic modulus of FRP bars was considered using the stiffness factor which depends on the shear span-to-reinforcement depth ratio and strain in the longitudinal FRP bars. In an experimental study, the strut efficiency coefficients required for calculating effective concrete strength in STM for steel-RC were experimentally validated for GFRP-RC members (Mohamed et al., 2016, 2017). In total 12 GFRP-RC beams were tested and verified against the existing models for GFRP-RC (i.e., CSA S806-12 (CSA, 2012)) and steel-RC (i.e., ACI 318-11 (ACI, 2011)). The average test-to-predicted ratio using STM in CSA S806-12 was calculated equal to 1.8 (CSA S806, 2012; Mohamed et al., 2016). The STM in ACI 318-11 over-estimated the capacity with an average test-to-predicted ratio equal to 0.99 (Mohamed et al., 2016). A similar over-prediction of STM in ACI 318-14 and ACI 318-19 has been reported in the literature with a test-to-predicted ratio equal to 0.88 for continuous GFRP-RC beams (Zinkaah et al., 2019; Zinkaah and Ashour, 2019). However, identical results have been reported in the cases of steel-RC deep beams as well for STM models in ACI 318 Code (Reineck et al., 2014; Tuchscherer et al., 2014). Therefore, the quality of the prediction may not be attributed to changing reinforcement types. The STM for steel-RC in ACI 318-19 (ACI, 2019) when applied to GFRP-RC squat walls resulted in an average test-to-predicted ratio equal to 1.02 (Shabana et al., 2023). Based on the above experimental and analytical studies, it seems reasonable to use the same STM model for GFRP-RC members as used for steel-RC in ACI 318-19 (ACI, 2019). It should be noted that STM in ACI 318-19 are force equilibrium based, and do not involve direct calculation of strains in the reinforcement, as otherwise in the case of CSA S806-12. The capacities of struts and nodes are governed by efficiency and confinement factors which depend on the location and confinement provided by surrounding concrete. The overestimation of capacities as reported in some cases using STM in ACI 318-14 or ACI 318-19 for GFRP-RC members may be addressed by modifying efficiency

factors based on the available literature. However, this paper only serves as an analytical approach based on previous studies to provide the framework for the adoption of STM for GFRP-RC members. Any deficiencies highlighted may be addressed by the Code committee with safety factors.

The ACI 318-19 (ACI, 2019) and ACI committee 445.2 (ACI, 2021) allow STM design of footings. Accordingly, in this study, an isolated footing was first designed with the provisions of ACI 440.11-22 (ACI, 2022) Chapters 13, 7, and 8 and subsequently with STM as per ACI 318-19 (ACI, 2019) Chapter 23. A comparison between the 2 design approaches is provided to highlight the differences in the final design and the necessity of adopting STM for GFRP-RC deep members in the next edition of ACI 440.11-22.

## 2 Methodology

In this study, a footing example from the ACI Reinforced Concrete Design Handbook (ACI 318-19, 2019) a Companion to ACI 318-19 (ACI, 2019) was selected and redesigned using GFRP reinforcement. The isolated footing supports the load from the  $610 \times 610$  mm<sup>2</sup> column as shown in Fig. 2, where  $b_1$  and  $b_2$  are the length and width of the footing ( $b_1 = b_2$  in this footing) and  $h$  is the thickness (as given in ACI Design Handbook (ACI 318-19 2019)). The constituent materials selected for the footing design are shown in Table 1. The concrete strength  $f'_c$  is 28 MPa while the GFRP bars are compliant with material specifications listed in ASTM D7957 (ASTM, 2022). The mechanical properties of GFRP bars affecting design include guaranteed ultimate tensile strength  $f_{frp}$  corresponding ultimate strain  $\epsilon_{frp}$  modulus of elasticity  $E_f$  and modular ratio  $n_f$ . A value of 1.20 for the bond coefficient,

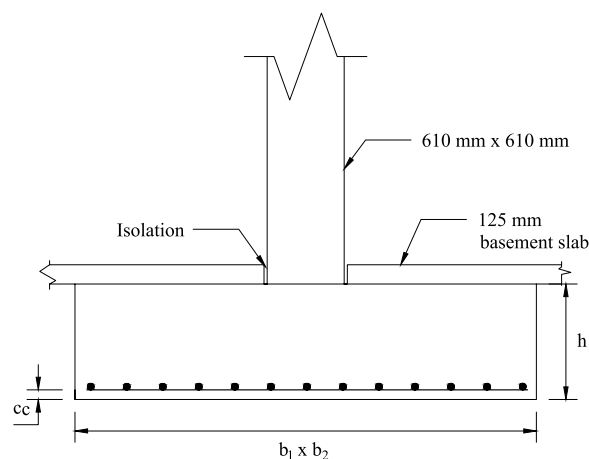


**Fig. 2** Square footing [ACI 318-19 Design Handbook (ACI 318-19, 2019)]

**Table 1** Properties of GFRP reinforcement, concrete, and soil

| Designation           | Nominal diameter (mm) | Nominal area (mm <sup>2</sup> ) | Elastic modulus (MPa) | Guaranteed tensile strength (MPa) | Ultimate strain (%) | Concrete strength (MPa) | Concrete clear cover (mm) | q <sub>(D+L)</sub> (kN/m <sup>2</sup> ) |
|-----------------------|-----------------------|---------------------------------|-----------------------|-----------------------------------|---------------------|-------------------------|---------------------------|---|
| GFRP-M29              | 28.6                  | 645                             | 44,815                | 565                               | 0.013               | –                       | 76                        | –                                       |
| Concrete strength     | –                     | –                               | –                     | –                                 | –                   | 28                      | –                         | –                                       |
| Soil bearing capacity | –                     | –                               | –                     | –                                 | –                   | –                       | –                         | 268                                     |

k<sub>b</sub>, and 0.85 for the environmental reduction factor, C<sub>E</sub>, are adopted as indicated in ACI 440.11-22 (ACI, 2022), Sects. 24.3.2.3 and 20.2.2.3, respectively. A concrete cover, c<sub>c</sub>, of 76 mm, is used as specified in ACI 440.11-22 (ACI, 2022) Sect. 20.5.1.3.1. The soil bearing capacity for the dead and live load (q<sub>D+L</sub>) was 268 kN/m<sup>2</sup> as given in the ACI Reinforced Concrete Design Handbook (ACI 318-19, 2019).

The footing was first designed with GFRP reinforcement using ACI 440.11-22 (ACI, 2022). Later, the same footing was redesigned using STM as per provisions in ACI 318-19, Chapter 23. The strut and node efficiency coefficients required for calculating effective concrete strength were taken from Tables 23.4.3a, 23.4.3b, and 23.9.2. The design of ties was carried out as per the procedure given in ACI 318-19, Sect. 23.8, and additionally, environmental reduction factor, bond factor, and strength reduction factors were adopted from ACI 440.11-22 (ACI, 2022). The anchorage of tie reinforcement is required as per ACI 318-19, Sect. 23.8.2 by mechanical devices, post-tensioning anchorage devices, standard hooks, or straight bars. For anchorage of GFRP reinforcement in this example, straight bars were used with development length calculated as per ACI 440.11-22, Chapter 25.

### 3 Design of GFRP-RC Shallow Foundation as Per Flexural Theory Approach (ACI 2022)

#### 3.1 Code Requirements

The footing carried a dead load equal to 2,406 kN and a live load 863 kN. These loads were combined as per ASCE 7-16 (ASCE, 2016) to compute the maximum factored demand. For applicable factored load combinations, design strength at all sections shall satisfy the requirements of ACI 440.11-22 (ACI, 2022), Sect. 9.5.1.1 as given below.

$$\Phi S_n \geq U \tag{1}$$

Strength reduction factor Φ was calculated as per ACI 440.11-22 Sect. 21.2.1 as given in Table 2.

The maximum spacing of GFRP reinforcement is limited as specified by ACI 440.11-22 (ACI 2022), Sects. 24.3.2a and 24.3.2b as given below.

**Table 2** Strength reduction factor Φ (ACI 440.11-22 (ACI 2022), Sect. 21.2.1)

| Action or structural element  | Φ             |
|---|---------------|
| Moment, axial force or combined axial moment and axial force (Sect. 21.2.2) | 0.55 to 0.65* |
| Shear   | 0.75          |

0.65 is applicable to over-reinforced sections used in this example

$$S \leq \frac{0.81E_f}{f_{fs}k_b} - 2.5c_c \tag{2}$$

$$S \leq 0.66 \frac{E_f}{f_{fs}k_b} - 2.5c_c \tag{3}$$

The development length of the GFRP reinforcement is governed by the code Sect. 25.4.2.1, as the greater of Eq. 4, 5, and 6 as given below.

$$l_d = \frac{d_b \left( \frac{f_{fr}}{0.083\sqrt{f_c}} - 340 \right)}{13.6 + \frac{c_b}{d_b}} \omega \tag{4}$$

$$20d_b \tag{5}$$

$$300mm \tag{6}$$

The reinforcement area shall be provided as greater of area required by the ultimate factored moment demand and area necessary to ensure that the flexural strength exceeds the cracking strength, indicated in ACI 440.11-22 (ACI, 2022), Sects. 9.6.1.2a and 9.6.1.2b as given below.

$$\frac{0.41\sqrt{f_c}}{f_{ju}} bd \tag{7}$$

$$\frac{2.3}{f_{ju}} bd \tag{8}$$

To avoid diagonal compression failure in GFRP-RC members maximum shear should be limited by Eq. 22.5.1.2 in ACI 440.11-22 (ACI 2022) as given below.

$$V_u \leq \Phi 0.2f'_c bd \tag{9}$$

The nominal shear strength can be calculated as per ACI 440.11-22 (ACI 2022), Sect. 22.5.1.1 given as:

$$V_n = V_c + V_f \tag{10}$$

The one-way shear strength provided by concrete was calculated as the greater of two expressions from ACI 440.11-22 (ACI 2022), Sects. 22.5.5.1a and 22.5.5.1b as given below.

$$V_c = 0.42\lambda_s k_{cr} \sqrt{f'_c} bd \tag{11}$$

$$V_c = 0.066\lambda_s \sqrt{f'_c} bd \tag{12}$$

$$k_{cr,rect} = \sqrt{2\rho_f n_f + (\rho_f n_f)^2} - \rho_f n_f \tag{13}$$

$$\rho_f = \frac{A_f}{bd} = \text{Reinforcement ratio}$$

$$n_f = \frac{E_f}{E_c} = \text{Modular ratio}$$

$E_c$  = Modulus of elasticity of concrete, MPa, calculated as given by the code Sect. 19.2.2.1

$$E_c = 4,700 \sqrt{f'_c} \tag{14}$$

$\lambda_s = \sqrt{\frac{2}{1+0.004d}}$  = Size effect factor as given in ACI 440.11-22, Sect. 22.5.1.1. The size effect factor should be considered for member depths greater than 300 mm. However, for footing design size effect factor can be taken equal to 1.0 as permitted in ACI 440.11-22 (ACI, 2022), Sect. 13.2.6.2.

Similarly, two-way shear strength was calculated as maximum of strength calculated with Eqs. 22.6.5.2a and 22.6.5.2b as given below:

$$v_c = 0.83\lambda_s k_{cr} \sqrt{f'_c} \tag{15}$$

$$v_c = 0.13\lambda_s \sqrt{f'_c} \tag{16}$$

### 3.2 Analysis and Design

The footing is considered a shallow foundation because its bottom is located 0.91 m below the basement slab (i.e., original footing given in ACI Reinforced Concrete Design Handbook (ACI 318-19, 2019)). The square footing is re-designed with applicable code provisions for one-way

slabs and two-way slabs as stated in the ACI 440.11-22 (ACI, 2022), code Sect. 13.3. The minimum base area of the shallow foundation was selected to satisfy the code requirements in Sect. 13.3.1.1, which requires that the minimum base area of the foundation shall be proportioned not to exceed the permissible bearing pressure when subjected to forces and moments applied to the foundation. It was observed that with applicable load combinations and allowable soil capacity, the minimum required base area of footing was 12.2 m<sup>2</sup>. Therefore, it was decided to use a 3.6 × 3.6 m<sup>2</sup> foundation that slightly exceeds the required dimensions. The dimensions of the footing and critical section for one-way and two-way shear verification are shown in Fig. 3, where  $b_1$  and  $b_2$  are the length and width of footing ( $b_1 = b_2$  for this case of square footing),  $b'_1$  and  $b'_2$  are the critical perimeter dimensions for two-way shear ( $b'_1 = b'_2$  for this case of square column). Also, shown are the critical sections for one-way shear (i.e., at a distance  $d$  from the column face) and two-way shear (i.e., at a distance  $d/2$  from the column face), and  $c_1$  and  $c_2$  are column dimensions (i.e., 610 mm × 610 mm as provided in ACI 318-19 Reinforced Concrete Design Handbook (ACI 318-19, 2019)).

The column does not impart a moment to the footing so that the soil pressure under the footing is uniformly distributed. The ACI 440.11-22 (ACI, 2022), Sect. 13.2.6.2 states that for one-way shallow foundations and two-way isolated footings, it is permissible to neglect the size effect factor specified in Sect. 22.5 and 22.6 for one-way and two-way shear provisions, respectively. Consequently, the size effect factor was neglected in both

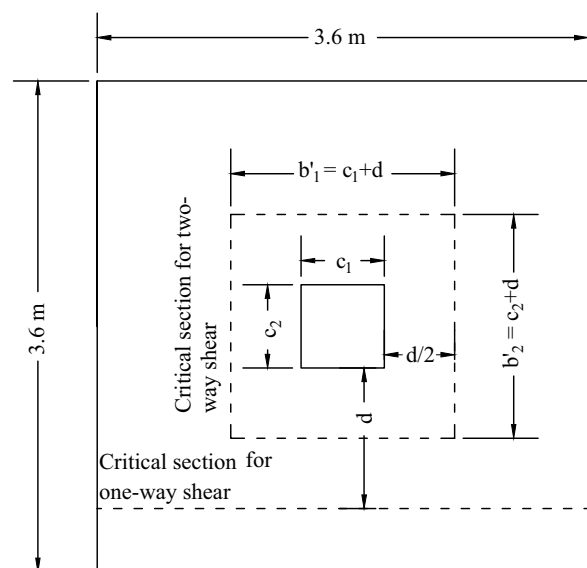


**Fig. 3** Square footing, column dimensions and critical sections for one-way and two-way shear

**Table 3** Design of steel-RC and GFRP-RC footing as per ACI 318-19 (ACI 2019) and ACI 440.11-22 (ACI 2022)

| Quantity                 | Steel-RC ACI 318-19 (ACI 2019) |               |            |               |            |       | GFRP-RC ACI 440.11-22 (ACI 2022) |            |               |            |                                 |               |            |
|--------------------------|--------------------------------|---------------|------------|---------------|------------|-------|----------------------------------|------------|---------------|------------|---------------------------------|---------------|------------|
|                          | h (m)                          | Demand        |            | Capacity      |            | h (m) | Demand                           |            | Capacity      |            | $\frac{A_{s, req}}{A_{s, pro}}$ | Moment (kN-m) | Shear (kN) |
|                          |                                | Moment (kN-m) | Shear (kN) | Moment (kN-m) | Shear (kN) |       | Moment (kN-m)                    | Shear (kN) | Moment (kN-m) | Shear (kN) |                                 |               |            |
| One-way shear            | 0.91                           | -             | 850        | -             | -          | 1.12  | -                                | 578        | -             | -          | -                               | 986           |            |
| Two-way shear            |                                | -             | 3651       | -             | -          |       | -                                | 3413       | -             | -          | -                               | 3,488         |            |
| Flexural strength (kN-m) |                                | 1,356         | -          | 2,045         | 0.85       |       | 1,356                            | -          | 3,074         | 0.58       |                                 | -             |            |

calculations, and it was assumed that shear strength is only provided by the concrete cross-section.

The critical section was assumed at distance  $d$  for one-way and  $d/2$  for two-way shear from the face of the column. The tributary area contributing to one-way shear and two-way shear were equal to 2.47 m<sup>2</sup> and 10.7 m<sup>2</sup>, respectively. The  $k_{cr}$  value was first calculated using a reinforcement ratio ( $\rho_f$ ) of 0.005 and a modular ratio ( $n_f$ ) 1.8, resulting equal to 0.11. (Note:  $\rho_f=0.005$  was adopted to meet both strength and serviceability requirements). However, the code section R22.5.5.1 requires a lower bound of 0.16 on the value of  $k_{cr}$  (i.e.,  $k_{cr}=0.16$ ) in the Eq. 22.5.5.1b (ACI 2022; Nanni et al., 2014); hence, this value was used to calculate one-way shear strength.

Ignoring the size effect factor and using normal-weight concrete, the GFRP-RC footing required a larger thickness for one-way shear than its steel-RC counterpart subjected to the same loads (i.e., 0.94 m, vs. 0.91 m). Using  $h=0.94$  m, the one-way shear strength of GFRP-RC footing calculated as per ACI 440.11-22 (ACI, 2022), Sects. 22.5.5.1a and 22.5.5.1b was equal to 815 kN which exceeds the demand of 786 kN.

Using  $h=0.94$  m, the two-way shear strength was calculated as per Sect. 22.6 resulting equal to 2565 kN which was less than demand of 3590 kN. Hence, the concrete cross-section thickness was increased to 1.12 m to satisfy two-way shear requirements. As shown in Table 3, the two-way shear strength at a thickness equal to 1.12 m is 3488 kN which is greater than the demand of 3413 kN. It should be noted that the 2-way shear strength for the steel-RC is 5902 kN at a thickness equal to 0.91 m as also shown in Table 3.

The critical section for the maximum bending moment was assumed at the face of the column as shown in Fig. 4. The tributary area contributing to the moment was equal to 5.4 m<sup>2</sup> and the ultimate moment calculated was equal to 1,356 kN-m. The reinforcement area used was the greater of the value required to resist the ultimate moment and minimum reinforcement value stated in Sects. 9.6.1.2a and 9.6.1.2b. This resulted in a value equal to 0.011 m<sup>2</sup>; however, to meet serviceability requirements stated in the ACI 440.11-22 (ACI 2022), Sects. 24.3.2a, 24.3.2b and 24.3.2.2, the reinforcement area was increased to 0.019 m<sup>2</sup> shown in Table 3 as the ratio of required and provided reinforcement area. In this footing design, M29 bars were placed at 127 mm c/c. The flexural capacity of GFRP-RC footing designed as per ACI 440.11-22 (ACI 2022), was equal to 3074 kN-m. The reinforcement area for steel-RC footing was equal to 0.007 m<sup>2</sup> and its moment capacity was 2045 kN-m (see Table 3). A sketch of dimensions and reinforcement details of GFRP-RC footing designed as per ACI 440.11-22 (ACI, 2022), are provided in Fig. 5.

The minimum length required for the anchorage of GFRP reinforcement was calculated as per Sect. 25.4.2.1, ACI 440.11-22 (ACI, 2022), for a bar diameter of 29 mm. The bar location modification factor ( $w$ ) was taken equal to 1.0 for tension reinforcement placed at 76 mm from the base of the footing. The development length calculated as per Sect. 25.4.2.1, Eq. 25.4.2.1a was equal to 1.38 m, which was greater than those calculated with Eq. 25.4.2.1b and 25.4.2.1c. Therefore, the value of 1.38 m obtained from Eq. 25.4.2.1a was adopted in the footing design as per ACI 440.11-22 (ACI, 2022). The development length calculated equal to 1.38 m must be provided in the footing to develop the full capacity of the section at the point of maximum moment. The development length required for GFRP-RC as per ACI 440.11-22 is 92% more than that required for steel-RC which is 0.72 m. In the current design example, the footing dimensions are 3.6 m × 3.6 m, hence bars can develop their full tensile capacity at the face of column (i.e., point of maximum moment). However, for footings of limited dimensions such as strip and wall footings detailing reinforcement for development length may be challenging.

The GFRP-RC shallow foundation required more reinforcement area than steel-RC and higher thickness. The extra materials and excavation costs may impose limitations on its application. Since the current design example has an  $a/d$  ratio equal to 1.84 using STM is justifiable compared to the conventional shear ( $V_c + V_s$ ) approach given in ACI 440.11-22 code (ACI, 2022).

#### 4 Design of GFRP-RC Footing Using STM (ACI, 2019)

This part of the study was carried out using STM in ACI 318-19 (ACI, 2019) for the design of struts and nodes. Ties were designed with same approach as given in ACI 318-19 (ACI, 2019) with modifications such as environmental reduction factor,  $C_E$ , bond factor,  $k_b$ , were adopted as given in ACI 440.11-22 (ACI, 2022). The GFRP-RC requires larger development lengths; hence the tie must be designed for proper anchorage as per provisions given in Chapter 25 of ACI 440.11-22 (ACI, 2022). The development length of GFRP-reinforcement was calculated as per ACI 440.11-22 (ACI, 2022), Sect. 25.4.2. GFRP properties, admissible soil pressure and concrete strength are considered the same as given in Table 1.

##### 4.1 Code Requirements

The ACI 318-19 (ACI, 2019) code Sect. 23.3 states that design strength of each strut, tie, and nodal zone in STM shall satisfy  $S_n \geq U$  including (a) through (c) given below:

- (a) Strut:  $\Phi F_{ns} \geq F_{us}$
- (b) Tie:  $\Phi F_{nt} \geq F_{ut}$

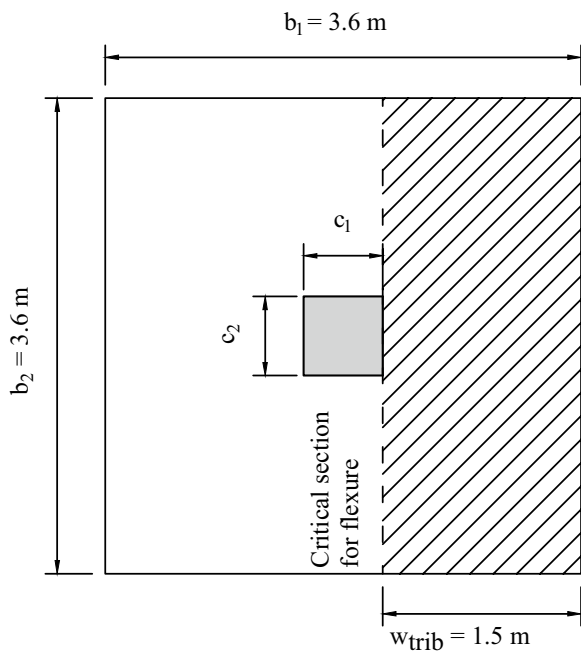


**Fig. 4** Critical section for the moment

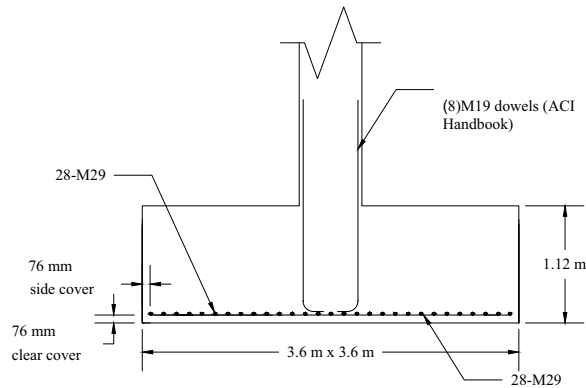


**Fig. 5** GFRP-RC Footing reinforcement detailing

(c) Nodal zones:  $\Phi F_{nm} \geq F_{us}$

$\Phi$  shall be calculated as per ACI 318–19 (ACI 2019), Sect. 21.2 (i.e., 0.75 as also suggested in ACI 445.2 guide for steel RC (ACI 2021)) for struts and ACI 440.11-22 (ACI, 2022), Sect. 21.2 for ties as provided in Table 2.

The nominal compressive strength of a strut,  $F_{ns}$ , shall be calculated as given in ACI 318-19 (ACI, 2019), code Sect. 23.4.1(a) or 23.4.1(b) as given below:

(a) Strut without longitudinal reinforcement

$$F_{ns} = f_{ce}A_{cs} \tag{17}$$

(b) Strut with longitudinal reinforcement

$$F_{ns} = f_{ce}A_{cs} + f_s'A_s' \tag{18}$$

It should be noted that ACI 318-19 (ACI, 2019), Sect. 23.4 states that  $F_{ns}$  shall be evaluated at each end of strut and taken as lesser value between strut and node.

Effective compressive strength of concrete in a strut  $f_{ce}$  shall be calculated in accordance with ACI 318-19 (ACI, 2019), Sect. 23.4.3 as given below:

$$f_{ce} = 0.85\beta_s\beta_c f'_c \tag{19}$$

where strut coefficient  $\beta_s$  and strut and node confinement modification factor  $\beta_c$  can be calculated in accordance with ACI 318–19 (ACI 2019), code Sect. 23.4.3a and 23.4.3b as given below in Tables 4 and 5:

The nominal tensile strength of a tie,  $F_{nt}$ , shall be calculated as given in the ACI 318-19 (ACI 2019), Sect. 23.7.2 as given below:

$$F_{nt} = A_{ts}f_{tu} \tag{20}$$

The nominal compressive strength of nodal zone,  $F_{nm}$ , shall be calculated as given in the ACI 318-19 (ACI, 2019), code Sect. 23.9 and given below:

$$F_{nm} = f_{ce}A_{nz} \tag{21}$$

**Table 4** Strut coefficient  $\beta_s$  (ACI 318-19 (ACI 2019), Sect. 23.4.3(a))

| Strut location                              | Strut type      | Criteria  | $\beta_s$ |     |
|---|-----------------|---|-----------|-----|
| Tension members or tension zones of members | Any             | All classes   | 0.4       | (a) |
| All other cases                             | Boundary struts | All cases   | 1.0       | (b) |
|   |                 | Reinforcement satisfying (a) or (b) of Table 23.5.1 | 0.75      | (c) |
|   | Interior struts | Located in regions satisfying 23.4.4                | 0.75      | (d) |
|   |                 | Beam-column joints                                  | 0.75      | (e) |
|   | All other cases |   | 0.4       | (f) |

**Table 5** Strut and node confinement modification factor  $\beta_c$  (ACI 318-19 (ACI 2019), Sect. 23.4.3(b))

| Location   | $\beta_c$ |  |     |
|--|-----------|--|-----|
| • End of a strut connected to a node that includes a bearing surface | Lesser of | $\sqrt{\frac{A_2}{A_1}}$ , where $A_1$ is defined by the bearing surface | (a) |
| • Node that includes a bearing surface                               |           |  | (b) |
| Other cases  | 1.0       |  | (c) |

**Table 6** Nodal zone coefficient  $\beta_n$  (ACI 318–19 (ACI 2019), Sect. 23.9.2)

| Configuration of nodal zone                          | $\beta_n$ |     |
|--|-----------|-----|
| Nodal zone bounded by struts, bearing areas, or both | 1.0       | (a) |
| Nodal zone anchoring on a tie                        | 0.80      | (b) |
| Nodal zone anchoring on one or more ties             | 0.60      | (c) |

Effective strength of concrete ( $f_{ce}$ ) at a face of nodal zone shall be calculated as given in the ACI 318-19 (ACI, 2019), Sect. 23.9.2 as given below:

$$f_{ce} = 0.85\beta_c\beta_n f'_c \tag{22}$$

where nodal zone coefficient  $\beta_n$  shall be calculated as given in ACI 318-19 (ACI, 2019), Sect. 23.9.2 provided in Table 6, and  $\beta_c$  as per 23.4.3(b) (i.e., Table 5).

The area of nodal zone  $A_{nz}$  can be calculated as given in Sect. 23.9.4 or 23.9.5. ACI 318-19 (ACI, 2019) code Sect. 23.9.4 states that area of nodal zone shall be taken as smaller of (a) and (b) given below:

- (a) Area of the face of nodal zone perpendicular to the line of action of  $F_{us}$
- (b) Area of a section through the nodal zone perpendicular to the line of action of the resultant force on the section

ACI 318-19 (ACI, 2019), Sect. 23.9.5 describes the area of a nodal zone in a three-dimensional strut-and-tie model as area of each face of nodal zone shall be at least that given in 23.9.4, and the shape of each face of the nodal zone shall be similar to the shape of the projection of the end of the strut onto the corresponding face of the nodal zone.

ACI 318-19 (ACI, 2019), Sect. 23.4.4 requires the minimum dimensions of a member shall be selected to preclude diagonal tension failure by imposing a limit on maximum shear as given below.

$$V_u \leq \phi 5 \tan \theta \lambda_s \sqrt{f'_c} b d \tag{23}$$

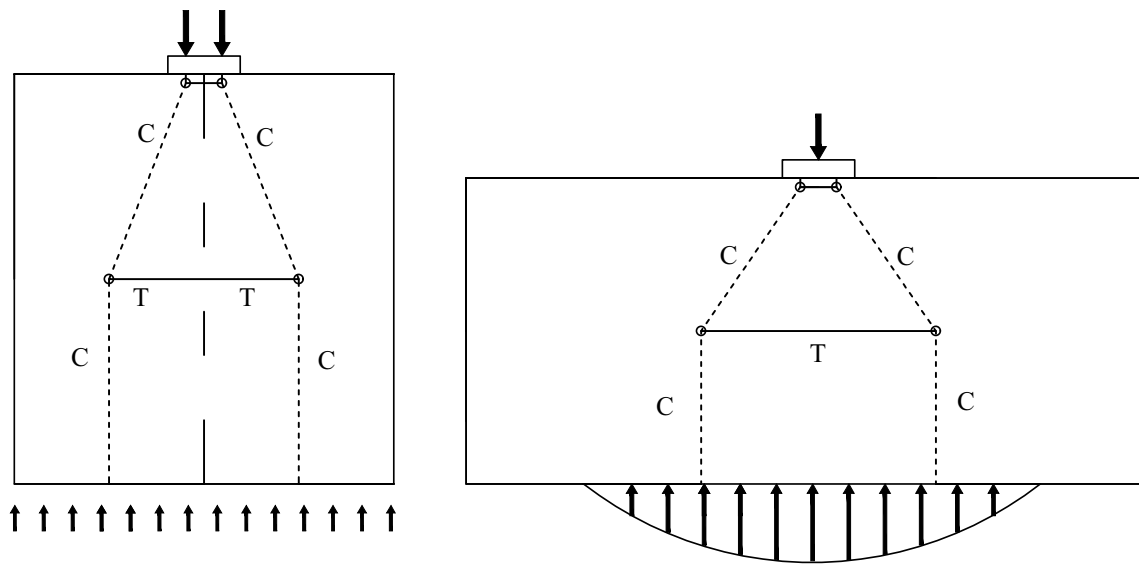
## 4.2 Analysis and Design

### 4.2.1 STM Dimensioning

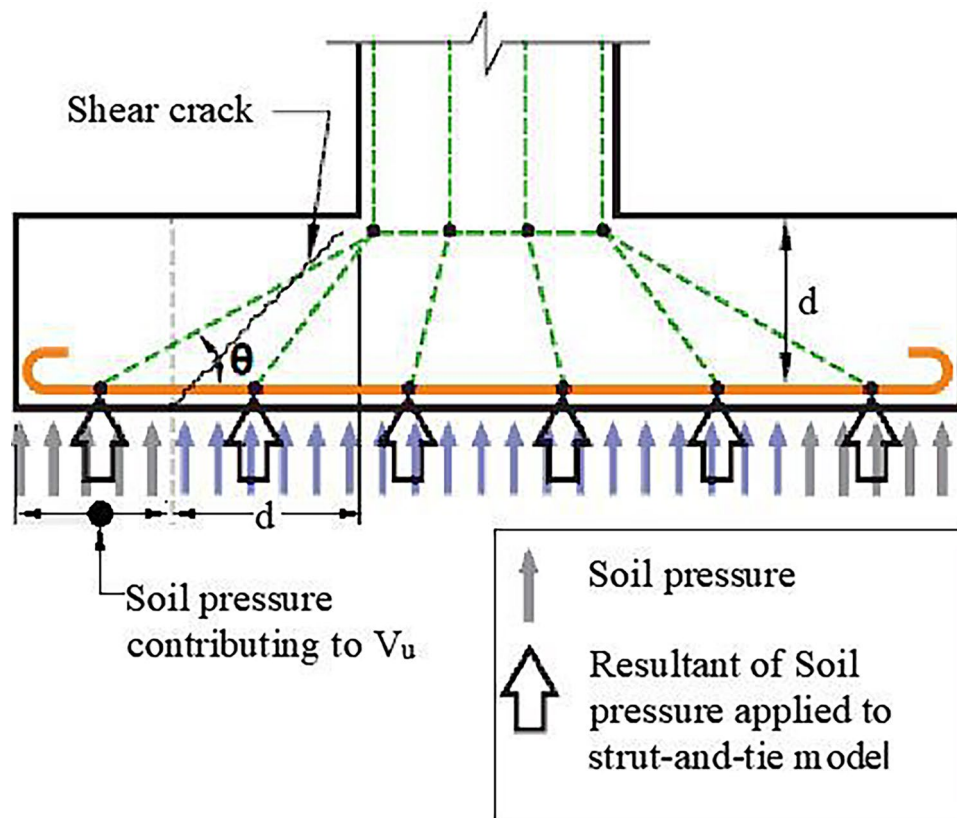
The various steps involved in the geometric layout of STM are effective concrete strength, shape and strength of struts, strength and anchorage of ties, and detailing requirements. In STM, it is important that struts do not cross each other, except at nodes and strength of each member exceeds the demand. Developing a STM of a D-region is much simplified if the elastic stresses and principal stress directions are available. Such an elastic analysis can be easily obtained from the wide variety of computer programs available today. The direction of struts can then be taken in accordance with the mean direction of principle compressive stresses or more important struts and ties can be located at the center of gravity of corresponding stress diagram. In the absence of any software the STM can be generated using the load path method (Schlaich et al., 1987). Depending on the dimensions of footing the number and direction of diagonal struts varies. Figs. 6 and 7 show the typical distribution of uniformly distributed loads to equivalent concentrated loads for strut and tie models.

Fig. 7 is taken from ACI 318–19, Chapter 13 where code allows to replace soil pressure with equivalent concentrated loads. A similar approach was adopted for the current design example and a model produced for footing was selected by interpolation of existing models in the literature (Schlaich et al., 1987; MacGregor, 2002; ACI, 2021). The developed strut and tie model for current design example is shown in Fig. 8a and b (Note: Fig. 8b is section A-A, taken from Fig. 8a). In these figures, the struts are labeled with the letter “C” and dotted lines, and do not cross each other as suggested in the literature (ACI, 2019) and ties are labeled with letter “T”. The uniform soil pressure acting on the footing was replaced with equivalent concentrated loads acting at nodes joining struts and ties as shown in Fig. 8b.

The load at the top nodes was divided into four equal loads applied on four equal areas of the column:  $(610 \text{ mm} \times 610 \text{ mm}^2)/4 = 305 \times 305 \text{ mm}^2$  transferring it to 8 struts (as shown in Fig. 8a). Assuming the forces are acting at the center of each of these areas, the



**Fig. 6** Strut-and-tie models for uniformly distributed loads (Schlaich et al., 1987)



**Fig. 7** Distribution of soil pressure and equivalent concentrated loads (ACI 2019)

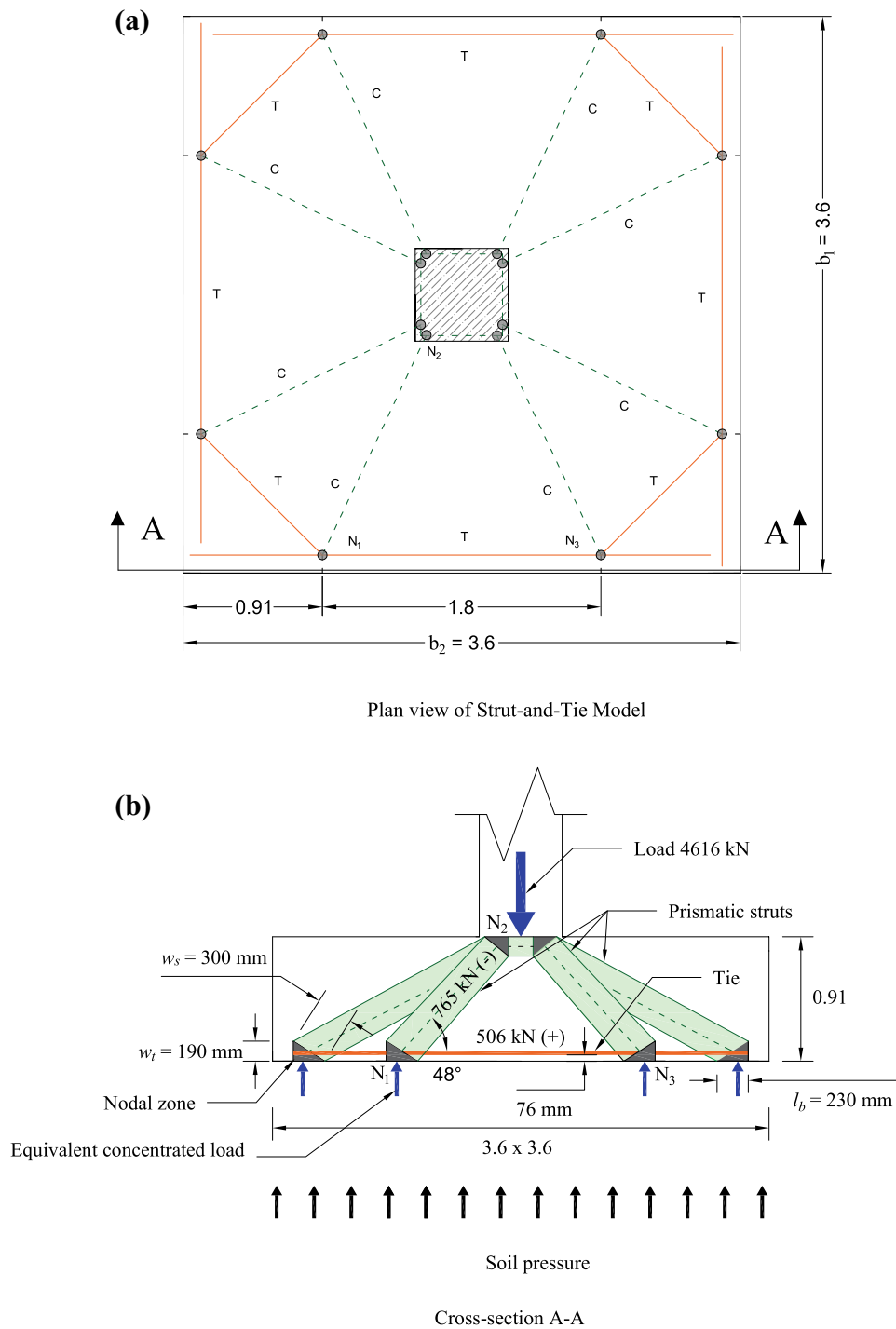


**Fig. 8** STM developed for current design example

maximum load on each of these areas was calculated equal to 1157 kN. The bottom node ( $N_1$ ) (i.e., intersection between strut-and-tie) is located at half of the tie width (i.e., 95 mm). The tie width was calculated following the recommendation in ACI 318-19 as also used

in the literature (ACI 318-19, Lim, E., and Hwang, S. J., 2016). The top node was located at 0.05 h ( $h = 914$  mm) from topmost surface of the footing (Macgregor, 2002). Usually these estimates are based on “back of the envelope” calculations. Minimum area of foundations is

still governed by the ACI 440.11-22 (ACI, 2022) code Sect. 13.3.1.1 (i.e.,  $3.6 \times 3.6 \text{ m}^2$ ) which states that minimum base area of foundation shall be proportioned to not exceed the permissible bearing pressure when subject to forces and moments applied to foundation (ACI, 2022). The horizontal and vertical projection of the nodes and corresponding forces in STM were calculated from the geometry of the model shown in Fig. 8a and b. The horizontal projection of Node 1 from end of footing is 914 mm, and vertical projection is at 190 mm from bottom. Whereas Node 2 is located at 1,981 mm from the left end and 870 mm vertically from bottom of the footing. The angle between the axis of strut-and-tie was calculated equal to 48 degrees. The axial force in the strut ( $S_1$ ) was calculated equal to 765 kN and that in the tie 506 kN as provided in Table 7. The width of prismatic diagonal strut was calculated equal to 300 mm. Since the footing designed is square and loads do not produce any moments hence only strut  $S_1$ , and tie  $T_1$  were analyzed and designed, remaining configuration will follow same loading and strength pattern. The calculated loads in STM are provided in Table 7 with negative sign implying compression.

The ACI 318-19 (ACI, 2019), Sect. 23.4.4 states that to preclude diagonal tension failure, the ultimate shear force (i.e.,  $V_u = 1157 \text{ kN}$ ) should be less than the limit provided in the code. Using the available dimensions ( $b = 3.6 \text{ m}$ , and  $d = 825 \text{ mm}$ ), the ultimate shear was less than the limit provided in the code (3900 kN). In the footing designed as per STM, the size effect factor was considered, and its value was calculated equal to 0.68 (as per Eq. 22.5.5.1.3). Note: Horizontal projection of nodes is from left end of footing, whereas vertical projection is from bottom.

ACI 445.2-21 (ACI, 2021) STM guidelines for ACI 318-19 (ACI, 2019) states to check two-way shear when designing foundations using STM. The shear-transfer capacity of STM depends on strut geometry and its inclination which is implicitly addressed in ACI 318-19 Sect. 23.4. This is also confirmed in recent publication by Shabana et al. (2023). Also, the authors assume that the requirements stated in ACI 445.2-21 guide for shear may be applicable to design boundary regions between

B-region and D-region, as D-regions can be completely analyzed using STM (Adebar et al. 1996). McGregor while developing derivation of STMs for the 2002 ACI code stated that for D-regions a different approach other than traditional B-region design methods (i.e., one-way, and two-way shear) is needed and proposed STM (Macgregor, 2002). Therefore, the authors solely focused on the provisions of ACI 318-19 (ACI, 2019), chapter 23 for STM models since  $a/d < 2.5$  for the current footing.

**4.2.2 Strength of Members**

*Strength of strut.* There are eight diagonal struts, all transferring loads of same magnitude. Hence, only one diagonal strut ( $S_1$ ), and one Tie ( $T_1$ ) as shown in Fig. 8 are presented. The strut  $S_1$ , transferred load equal to 765 kN to the node  $N_1$  joining strut  $S_1$  and tie  $T_1$ . The strut strength was calculated as per ACI 318-19 (ACI, 2019), Sect. 23.3. The effective concrete strength in strut  $S_1$  was calculated as per ACI 318-19 (ACI, 2019), Sect. 23.4.3. The efficiency factor for effective concrete strengths was calculated using Tables 23.4.3a and Table 23.4.3b of ACI 318-19 (ACI, 2019)

The efficiency factor of strut depends on load duration effects, cracking, strut type, transverse strains, and confinement from surrounding concrete. The strut efficiency co-efficient “ $B_s$ ” for an interior strut was taken from Table 23.4.3a of ACI 318-19 (ACI, 2019). It should be noted that the adopted STM satisfies the requirements stated in ACI 318-19 (ACI, 2019), Sect. 23.4.4 Table 23.4.3a. Also,  $S_1$  is an interior restrained strut (ACI, 2019), hence the strut efficiency factor was taken equal to 0.75 as given in Table 23.4.3(a) of ACI 318-19 (ACI, 2019). Further, due to three dimensions of the footing, strut strength should be greater due to confinement of surrounding concrete. Similarly, the confinement modification factor “ $B_c$ ” was conservatively taken equal to 1.0 from Table 23.4.3b. The strength reduction factor for the strut was taken equal to 0.75 as given in ACI 318-19 (ACI, 2019) and ACI 445.2–21 Strut-and-tie method guidelines for ACI 318–19- Guide (ACI, 2021).

Using the above parameters, the effective compressive strength of concrete in diagonal strut  $S_1$  was equal to

**Table 7** Geometry and Forces in the Struts and Tie

| Strut/Tie |       | Horizontal Projection (mm) | Vertical Projection (mm) | Angle (degrees) | Demand                  |                           |                  |
|-----------|-------|----------------------------|--------------------------|-----------------|-------------------------|---------------------------|------------------|
|           |       |                            |                          |                 | Vertical Component (kN) | Horizontal Component (kN) | Axial Force (kN) |
| $S_1$     | $N_1$ | 914                        | 190                      | 48              | 576                     | 506                       | – 765            |
|           | $N_2$ | 1981                       | 870                      |                 |                         |                           |                  |
| $T_1$     | $N_1$ | 914                        | 190                      | 0               |                         |                           | 506              |
|           | $N_3$ | 2743                       | 190                      | 0               |                         |                           |                  |

**Table 8** STM geometry of members, demand, and capacity

| Strut/Tie/Node | Angle (degrees) | Demand (kN) | Capacity (kN) |
|----------------|-----------------|-------------|---------------|
| S <sub>1</sub> | 48              | – 765       | 1180          |
| T <sub>1</sub> | 0               | 506         | 832           |
| N <sub>1</sub> | –               | – 576       | 963           |
| N <sub>2</sub> | –               | – 576       | 1595          |

17.5 MPa. The diagonal strut was assumed to be a square strut with each dimension calculated equal to 300 mm. Using strut dimensions, effective strength of concrete in the strut and strength reduction factor, the strut strength was calculated equal to 1180 kN, which is greater than demand 765 kN. The demand and capacity values of strut S<sub>1</sub> are provided in Table 8.

**Strength of Nodes.** A node consisting of strut, tie and bearing surface was represented as CCT node (N<sub>1</sub>). Whereas that with strut on two sides and a force or bearing surface on other side as CCC node (N<sub>2</sub>) as stated in ACI 318-19 (ACI, 2019), section R23.2.6. When checking the strength of a node, the smaller value of effective concrete strength between intersecting strut and node should be used in the design.

The strength of the node was calculated as per ACI 318-19 (ACI 2019) Sect. 23.9, and nodal zone coefficient “B<sub>n</sub>” was calculated as given in Table 23.9.2 (ACI, 2019). The nodal zone coefficient “B<sub>n</sub>” for a CCT node (i.e., N<sub>1</sub>) was taken equal to 0.8 as it anchors one Tie. Using node confinement modification factor equal to 1.0 as stated in Table 23.4.3b (ACI, 2019) and nodal zone coefficient equal to 0.8, the effective strength of concrete in Node N<sub>1</sub> (CCT) was equal to 18.7 MPa. The minimum width of bearing surface at node 1 required for applied vertical load (i.e., 576 kN) was calculated to be equal to 230 mm. It should be noted that the width of the bearing surface is usually governed by the bearing plate or support at the node. However, in the case of footing, the load from node is transferred to the soil. It could be assumed that bearing width (*l<sub>b</sub>*) is the tributary width contributing to concentrated load at the node (as in some wall examples with multiple ties within wall depth). However, for calculation purposes only the minimum required width to support the applied load was used (i.e., 230 mm). The thickness of node was taken equal to width of strut at node 1 (i.e., 300 mm). Using the above dimensions, effective concrete strength of node 1 and strength reduction factor, the bearing strength of Node 1 (N<sub>1</sub>) was calculated equal to 963 kN which is greater than demand 576 kN as shown in Table 8.

Similarly, the strength of node 2 (CCC) was calculated assuming diagonal strut (S<sub>1</sub>) having square cross-section

and its dimensions at Node 2 calculated equal to 300 mm. The width of node 2 was taken equal to width of bearing surface at node 2 (i.e., area transforming load to strut 1) and its thickness equal to width of strut. The node confinement modification factor “B<sub>c</sub>” was taken equal to 1.0 and nodal zone modification factor “B<sub>n</sub>” was equal to 1.0 as adopted from Table 23.9.2, ACI 318-19 (ACI, 2019). The effective strength of concrete for node 2 was calculated equal to 23.4 MPa. Using the above parameters, the strength of Node 2 (CCC) was equal to 1595 kN, which is greater than the demand of 576 kN. The demand and capacity values for Node 2 are provided in Table 8.

**Strength of Tie.** The thickness of the tie in this study was equal to 190 mm, and the width of tie was taken equal to width of the node 1 (i.e., 300 mm). As previously described the thickness of tie was calculated by dividing the force in the tie by efficiency and width of the node (Lim, E., and Hwang, S. J., 2016). The mechanical properties of GFRP reinforcement are given in Table 1. The required reinforcement area for the applied force 506 kN was equal to 1052 mm<sup>2</sup>. Therefore, 2-M29 bars were used at 125 mm (*A<sub>f</sub>*=1535 mm<sup>2</sup>) center-center-center spacing. The capacity of tension tie, T<sub>1</sub>, was equal to 832 kN which is greater than 506 kN (i.e., demand) as given in Table 8. The details of tie reinforcement and its detailing are provided in Fig. 9. ACI 318-19 (ACI, 2019) Sect. 23.8.3 requires that tie force shall be developed in each direction at the point where the centroid of reinforcement in the tie leaves the nodal zone. The development length required to develop the tie force was equal to 1.14 m which was provided by a straight, and a bent bar as shown in Fig. 9.

### 4.3 Secondary Reinforcement

The GFRP type used for secondary reinforcement was compliant with material specification ASTM D7957 (ASTM, 2022). The mechanical properties of GFRP bars affecting design are provided in Table 1. The minimum secondary reinforcement is required by ACI 440.11.22 (ACI, 2022), Sect. 24.4.3.2, which states that the ratio of shrinkage and temperature reinforcement area to gross area shall not be less than 140/E<sub>f</sub>. The minimum reinforcement area needed to satisfy the code requirements was equal to 0.009 m<sup>2</sup>. Therefore, a mat was used consisting of M29 bars spaced at 211 mm center-to-center parallel to each side of the square footing. The required shrinkage reinforcement could be adjusted for Tie reinforcement, hence the required reinforcement for shrinkage and temperature will reduce to M29 bars placed at 290 mm center-to-center as allowed in ACI 440.11 Code. The secondary reinforcement details are provided in Fig. 9.

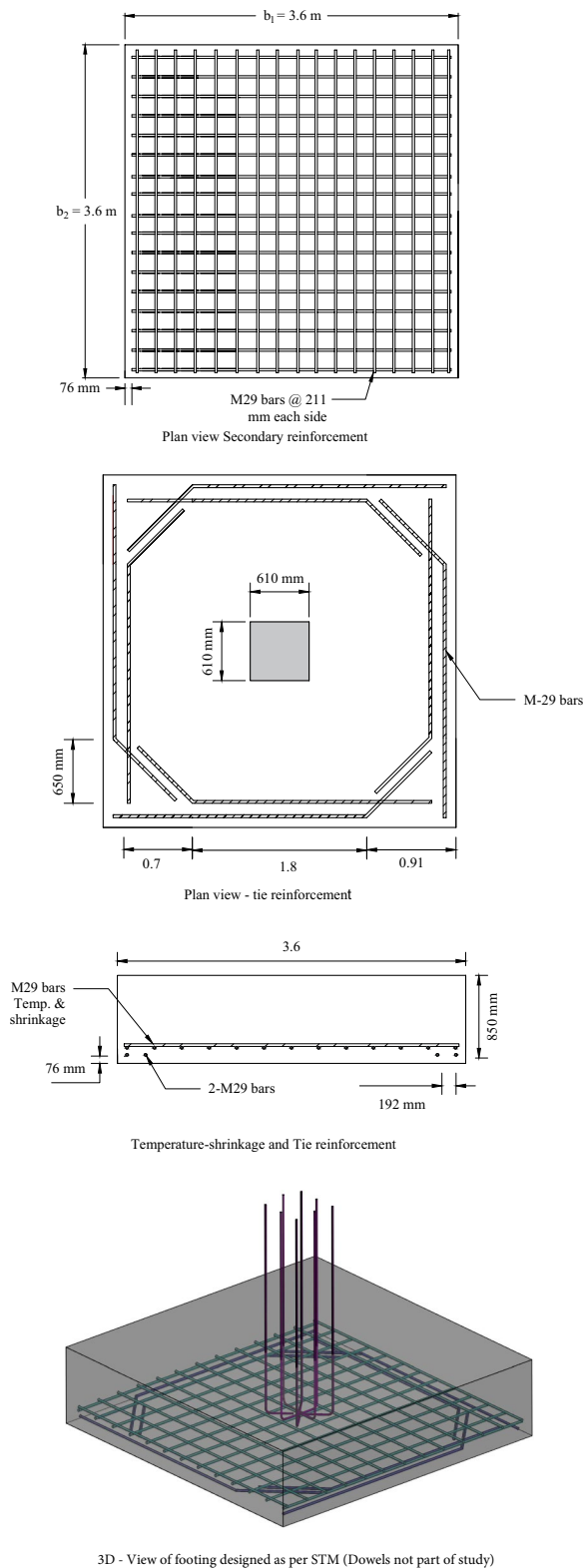


**Fig. 9** Reinforcement details of footing (designed as per STM)

The required shrinkage and temperature reinforcement is 80% more than that required for steel-RC which required  $0.005 \text{ m}^2$  (i.e., M29 bars at 365 mm c/c). The secondary reinforcement provisions in ACI 318-19 are based on an empirical approach which has been found to produce satisfactory results for steel-RC. The ratio of GFRP bar area-to-gross concrete area required by code Sect. 24.4.3.2 (ACI 2022) was intended to provide same force capacity as does the 0.0018 ratio required by ACI 318-19 (Shield et al., 2019). Further, a limit on maximum spacing of GFRP temperature and shrinkage reinforcement is also provided as lesser of the value obtained from 3 h or 300 mm. This limit is stricter than that required by steel-RC, which is minimum of 5 h or 460 mm. Accordingly, the secondary reinforcement provisions for GFRP-RC members impose a significantly larger reinforcement area. For example, in this study shrinkage and temperature reinforcement required as per ACI 440.11-22, Sect. 24.4.3.2 is equal to M29 bars at 211 mm center-to-center, which is more than half the amount required for strength and detailing (i.e., M29 bars @ 127 mm). Therefore, it is necessary to experimentally investigate the minimum reinforcement required for temperature and shrinkage for GFRP-RC members.

### 5 Conclusions and Recommendations

In this study, a footing example was taken from ACI Reinforced Concrete Design Handbook (ACI 318-19 2019), a Companion to ACI 318-19 (ACI, 2019) and redesigned with GFRP reinforcement to show the implication of some ACI 440.11-22 (ACI, 2022) building code provisions. Later, the footing was redesigned using strut-and-tie method as per guidelines of ACI 318-19 (ACI, 2019). The concrete strength  $f'_c$  was assumed to be 28 MPa and bond coefficient,  $k_b = 1.20$ , and environmental reduction factor,  $C_E = 0.85$  were used as per ACI 440.11-22 (ACI, 2022). Other assumptions regarding soil pressure and geometry of strut-and-tie model were also made.

Based on the outcomes of this study in the design and detailing, the following conclusions were drawn:

- The reinforcement area required for GFRP-RC footing was higher compared to steel-RC due to detailing requirements in ACI 440.11-22.
- GFRP-RC footing designed as per ACI 440.11-22 Building Code required a thickness value equal to 1.12 m, whereas that designed as per ACI 318-19 using steel reinforcement required 0.91 m.
- The required thickness GFRP-RC footing decreased to 0.91 m when designed using strut-and-tie method,

which is similar to steel-RC footing using ACI 318-19 sectional design approach.

- Based on analytical study and available literature strut-and-tie method is found to be a more promising way to design GFRP-RC footings when  $a/d$  is less than 2.5.
- The GFRP reinforcement requires longer development length which may be an issue in footings of limited dimensions when developing full tensile capacity at the face of node.
- Minimum secondary reinforcement was also provided in addition to that required for ties as required by ACI 440.11-22. The footing required M29-bars at 211 mm center-to-center, which is close to reinforcement requirements for strength and detailing.
- Based on the outcomes of this study, it is evident ACI 440.11 provisions for design of GFRP-RC deep members impart significant challenges to the designer. It is important to utilize innovative methods such as STM to ease such challenges. The literature agrees on fact that STM in ACI 318-19 closely estimates the capacities of GFRP-RC deep members. However, some discrepancies also exist in the literature about over-prediction of strength. Therefore, modifications in terms of safety factor or efficiency factors in ACI 318-19 may be carried out to address the issues highlighted in the literature. Thereby, a chapter addressing the use of STM for GFRP-RC may be added in the next edition of ACI 440.11-22 Code.

#### List of symbols

|          |  |
|----------|--|
| $A_{cs}$ | Cross-sectional area at the end of strut   |
| $A_{ns}$ | Area of face of nodal zone or a section through nodal zone, mm <sup>2</sup>  |
| $A'_s$   | Area of compression reinforcement at nominal axial strength of strut   |
| $A_{ts}$ | Area of reinforcement in a tie, mm <sup>2</sup>  |
| $A_f$    | Area of GFRP reinforcement within spacing $S$ , mm <sup>2</sup>  |
| $b$      | Web width or diameter of the circular cross-section, mm  |
| $c_b$    | Lesser of: (a) the distance from center of a bar to nearest concrete surface, and (b) one-half the center-center spacing of bars being developed, mm |
| $c_c$    | Concrete cover   |
| $d$      | Distance from extreme compression fiber to centroid of longitudinal tension reinforcement, mm  |
| $d_b$    | Nominal diameter of bar, mm  |
| $E_c$    | Modulus of elasticity of concrete, MPa   |
| $E_f$    | Modulus of elasticity of GFRP reinforcement, MPa   |
| $f'_c$   | Compressive strength of concrete at 28 days  |
| $F_{ce}$ | Effective strength of concrete   |
| $F'_s$   | Stress in the compression reinforcement at nominal axial strength of strut   |
| $f_{fr}$ | Tensile stress in GFRP reinforcement required to develop the full nominal section capacity, MPa  |
| $f_{fs}$ | Stress at service loads  |
| $F_{ns}$ | Nominal strength of strut, $N$   |
| $F_{nn}$ | Nominal strength at the face of nodal zone, $N$  |
| $F_{us}$ | Factored compressive force in a strut, $N$   |
| $F_{ut}$ | Factored tensile force in a tie, $N$   |
| $F_{fu}$ | Design tensile strength of GFRP reinforcement, MPa   |
| $k_b$    | Bond dependent coefficient   |
| $k_{cr}$ | Ratio of the depth of elastic cracked section neutral axis to the effective  |

|              |  |
|--------------|--|
|              | depth  |
| $M_u$        | Ultimate factored moment at a section, kN-m  |
| $S_n$        | Nominal moment, shear, axial or torsional strength   |
| $S_{max}$    | Maximum allowed spacing, mm  |
| $U$          | Strength of a member or cross section required to resist factored loads or related internal moments and forces |
| $V_c$        | Nominal shear strength provided by the concrete, $N$   |
| $V_f$        | Nominal shear strength provided by GFRP shear reinforcement, $N$   |
| $V_n$        | Nominal shear strength, $N$  |
| $V_u$        | Factored shear force at section, $N$   |
| $W_u$        | Ultimate factored load, kN/m   |
| $\omega$     | Bar location modification factor   |
| $\epsilon_f$ | Strain in GFRP flexural reinforcement  |
| $\Phi$       | Strength reduction factor  |

#### Acknowledgements

The authors would like to acknowledge the National Science Foundation (NSF), for funding the lead author under Grant Number 1916342.

#### Author contributions

ZH: Conceptualization, methodology, investigation, analysis, writing. AN: Conceptualization, methodology, analysis, review.

#### Funding

The authors would like to thank the National Science Foundation (NSF), for funding the lead author.

#### Data availability

All data generated or analyzed during the current study are included in this manuscript.

#### Declarations

#### Competing interests

The authors declare that they have no known competing interests or personal relationships that could have appeared to influence the work reported in this paper.

Received: 3 September 2023 Accepted: 11 March 2024

Published online: 11 July 2024

#### References

- ACI (American Concrete Institute). (2011). *Building code requirements and commentary*. ACI 318–11. Farmington Hills, MI: ACI.
- ACI (American Concrete Institute). (2019). *Reinforced concrete design handbook: A companion to ACI 318–19*. Farmington Hills, MI.
- ACI (American Concrete Institute). (2019). *Building code requirements for structural concrete (ACI 318–19) commentary on building code requirements for structural concrete (ACI 318R–ACI 318–19)*. Farmington Hills, MI: ACI.
- ACI (American Concrete Institute). (2021). *Strut-and-Tie method guidelines for ACI 318–19 – Guide*. 445.2–21. Farmington Hills, MI: ACI.
- ACI (American Concrete Institute). (2022). *Building code requirements for structural concrete reinforced with glass fiber-reinforced polymer (GFRP) bars-code and commentary*. ACI 440.11-22. Farmington Hills, MI: ACI.
- Adebar, P., & Zhao, L. (1996). Design of deep pile caps by Strut-and-Tie models. *ACI Structural Journal*, 93(4), 1–12.
- ASCE (American Society of Civil Engineers). (2016). *Minimum design loads and associated criteria for buildings and other structures*. ASCE 7–16. Reston Virginia. ASCE.
- ASTM (American Society of Testing Materials). (2022). *Standard specifications for solid round glass fiber reinforced polymer bars for concrete reinforcement*. ASTM D7957/D7957M-22. West Conshohocken, PA: ASTM International.
- Collins, M. P., and Mitchel, D. (1991). *Prestressed concrete structures*. Prentice Hall, Englewood Cliffs, USA: NJ.
- CSA (Canadian Standard Association). (2012). *Design and construction of building structures with fiber reinforced polymers*. CSA S806–12. Mississauga, Ontario: CSA.

- Lim, E., and Hwang, S.J., (2016). Modelling of the strut-and-tie parameters of deep beams for shear strength. *Engineer Structures*, 108(2016), 104–112.
- Macgregor, J. G. (2002). Derivation of strut-and-tie models for 2002 ACI Code. *In Proceedings of ACI Fall Convention.*, 7–40. Phoenix Arizona.
- Mohamed, K., Farghaly, A., & Benmokrane, B. (2016). Strut efficiency-based design of concrete deep beams reinforced with fiber-reinforced polymer bars. *ACI Structural Journal*, 113(6), 1–9.
- Mohamed, K., Farghaly, A., Benmokrane, B., & Kenneth, W. N. (2017). Non-linear finite-element analysis for the prediction and strut efficiency factor of GFRP-reinforced concrete deep beams. *Engineering Structures*, 137, 145–161.
- Nanni, A., Luca, A. D., & Zadeh, J. J. (2014). *FRP reinforced concrete structures: mechanics and design*. CRC.
- Reineck, K. H., & Todisco, L. (2014). Database of shear tests for non-slender reinforced concrete beams without stirrups. *ACI Structural Journal*, 111(6), 1363–1372.
- Schlaich, J., Schafer, K., & Jennewein, M. (1987). Towards a consistent design of structural concrete. *PCI Journal*, 32(3), 74–150.
- Shabana, I., Farghaly, A. S., & Benmokrane, B. (2023). Shear strength of Glass fiber-reinforced polymer-reinforced concrete squat walls: Strut-and-tie-model. *ACI Structural Journal*, 120(2), 61–75.
- Shield, C., Brown, V., Bakis, C., & Gross, S. (2019). A recalibration of the crack width bond-dependent coefficient for GFRP-reinforced concrete. *Journal of Composites for Construction*, 23(4), 1–8. [https://doi.org/10.1061/\(ASCE\)CC.1943-5614.0000978](https://doi.org/10.1061/(ASCE)CC.1943-5614.0000978)
- Tuchscherer, R. R., Birrcher, D. B., William, C. S., Deschenes, D. J., & Bayrak, O. (2014). Evaluation of existing strut and tie models and recommended improvements. *ACI Structural Journal*, 111(6), 1451–1460.
- Zinkaah, O. H., & Ashour, A. (2019). Load capacity prediction of continuous deep beams reinforced with GFRP bars. *Structures*, 19(2019), 449–462.
- Zinkaah, O. H., Ashour, A., & Sheehan, T. (2019). Experimental tests of two-span continuous concrete deep beams reinforced with GFRP bars and strut-and-tie method evaluation. *Composite Structures*, 216(2019), 112–126.

## Publisher's Note

Springer Nature remains neutral with regard to jurisdictional claims in published maps and institutional affiliations.

**Zahid Hussain** is a PhD candidate in the Civil and Architectural Engineering Department at the University of Miami. He is a student member of ACI Committee 440, Fiber Reinforced Polymer Reinforcement. His research interests include sustainable materials, computational methods, design, and behavior of reinforced concrete structures.

**Antonio Nanni** is an Inaugural Senior Scholar, Professor, and Chair of the Department of Civil and Architectural Engineering at the University of Miami. He is a member of ACI Committee 549, Thin Reinforced Cementitious Products and Ferrocement, and ACI Committee 440, Fiber Reinforced Polymer Reinforcement.